A NOVEL CONTROL STRATEGY TO ENHANCE THE DYNAMIC RESPONSE OF THE WIND ENERGY CONVERSION SYSTEM USING A DOUBLY FED INDUCTION GENERATOR BASED ON AN INTELLIGENT FUZZY-PI CONTROLLER

Nguyen Thi Hue[1], Huynh Hoang Bao Nghia[2], Le Van Dai[2*]

[1]*Dong Nai Technology University*
[2]*Industrial University of Ho Chi Minh City*
*Corresponding author: *Le Van Dai, levandai@iuh.edu.vn*

GENERAL INFORMATION

Received date: 10/11/2024

Revised date: 03/01/2025

Accepted date: 08/01/2025

KEYWORD

Doubly fed induction generator (DFIG);

Dynamic response;

Fuzzy control;

Wind energy conversion system (WECS);

Proportional-integral (PI);

Simulation analysis.

ABSTRACT

This paper introduces a practical and simple power control method for wind energy conversion systems based on a doubly-fed induction generator. Due to the limitations of traditional proportional-integral controllers when the parameters of the doubly-fed induction generator and wind speed vary, fuzzy control theory is applied to overcome these challenges. First, a detailed mathematical model of the induction generator in the *dq* domain is provided. Then, based on the characteristics of the doubly-fed induction generator, an enhanced mathematical model is presented along with a vector control model for the generator. Subsequently, the mathematical model for the wind turbine and the fuzzy controller based on the proportional-integral controller are developed and implemented in MATLAB/Simulink for simulation and performance evaluation. Simulation results indicate that the proposed method for controlling the doubly-fed induction generator can significantly improve the dynamic response performance under varying generator parameters and wind speed conditions.

1. INTRODUCTION

The increasing global demand for electrical energy has intensified its influence on geopolitical issues, including economic and environmental concerns. Renewable energy sources such as wind, solar, and hydroelectric power are becoming critical solutions to meet current and future electricity demands worldwide (Le Dai, Pham, 2023). Among these, wind energy contributes approximately 24% to the global renewable energy mix as of 2023, making it one of the most promising sources of electricity generation (LV Dai, Tung, 2017; Hassan et al., 2024). Wind turbines (WTs), as a crucial component of wind energy conversion systems, are responsible for converting kinetic energy from wind into electrical energy, with modern turbine efficiencies reaching up to 50%. Over the years, advancements in wind turbine technologies have led to the development of three primary operational types: fixed-speed, semi-variable speed, and variable-speed turbines, with variable-speed systems achieving up to 30%

higher energy capture (Ackermann, 2012). One of the most widely used turbine-generator systems is based on doubly-Fed induction generators (DFIG), which are controlled by back-to-back power converters accounting for approximately 50% of installed wind farms globally, covering both onshore and offshore applications (Liserre, Cardenas, Molinas, & Rodriguez, 2011). DFIG-based wind energy conversion systems (DFIG-WECS) have gained significant attention due to their capability to handle wind speed variations between 4 m/s to 25 m/s efficiently and to control active and reactive power independently, maintaining a power factor close to unity (Mehdipour, Hajizadeh, & Mehdipour, 2016). Research on DFIG-WECS models has primarily focused on addressing wind speed variability, improving power quality, and enhancing system dynamics (Bensahila, et al., 2020; Boutoubat et al., 2013; Mehdipour et al., 2016). Several control techniques have been proposed to enhance the performance of wind energy systems: The study by (Abolhassani, et al., 2008) developed a WECS model to maximize wind power capture and improve power quality by reducing nonlinear harmonic currents by up to 90%. However, this model did not address reactive power compensation or overload in the rotor side converter (RSC), which is critical for grid integration. Research (Singh, Chandra, 2010) introduced a grid side converter (GSC) model that acted as an active filter, achieving harmonic compensation within 5% of IEC standards while maintaining a power factor above 0.98. Research (Jain, Ranganathan, 2008) proposed using the GSC in parallel operation for independent power grids, achieving voltage regulation within ± 5% under varying load conditions. The above approaches provide promising control theories, but there are still challenges in optimizing the control systems to improve reliability, scalability, and stability under different operating conditions. To address these gaps, this paper proposes a mathematical model of DFIG-WECS to study the ability to regulate the stator and rotor currents, ensuring stable output power under different wind conditions. The model demonstrates that the system can maintain output stability at wind speeds ranging from 6 m/s to 20 m/s, with power fluctuations limited to ± 3%. The rest of this paper is structured as follows: Section 2 discusses the theoretical framework of the WT generator model. Section 3 details the control system for DFIG-WECS. Section 4 presents the studies under different wind speed scenarios, followed by conclusions presented in Section 5.

2. WECS MODEL

The block diagram of the overall control system for the DFIG-WECS is illustrated in Fig. 1. It consists of two main parts: The first part is the electrical control system of the DFIG, which includes the RSC and the GSC. The objective of the RSC is to enable the DFIG WT to control active and reactive power or speed independently. Meanwhile, the GSC aims to maintain the DC link voltage at a specified value, regardless of the direction and magnitude of the rotor power. The second part is the mechanical control system of the WT, which primarily aims to achieve maximum wind power extraction and minimize low-speed load stresses. Therefore, controlling the DFIG-WECS system is essential and will be presented in the following subsection.

2.1. Wind Turbine

The presentation of the mechanical system of an entire WT is quite complex. For modeling and simulation, a two-mass drive model is proposed to study the dynamic stability of the electromechanical system, which is expressed by the following equations (LV Dai, Tung, 2017)

$$\begin{cases} J_t \dfrac{\partial \omega_t}{\partial t} = T_t - T_g \\ J_g \dfrac{\partial \omega_g}{\partial t} = T_g - T_t - D_g \omega_g \end{cases} \quad (1)$$

where; J_t is the turbine inertia constant, T_t is the turbine torque, T_g is the generator torque, ω_t is the turbine speed, J_g is the generator inertia constant, ω_g is the generator speed, D_g is the friction coefficient of the generator and P_m is the wind turbine mechanical power and is given as (Miller et al., 2003; Tohidi et al., 2016):

$$P_m = P_w C_p(\beta, \lambda) \quad (2)$$

The wind power swept can be converted depending on the air density ρ, β is the tip speed ratio, λ is the blade pitch angle, the turbine blade radius R, and the wind speed V_w, as (Yang et al., 2017):

$$P_w = \frac{1}{2}\rho\pi R^2 V_w^3 \quad (3)$$

The power coefficient can be defined as:

$$C_p(\beta, \lambda) = \sum_{i=0}^{4}\sum_{j=0}^{4} \alpha_{i,j}\beta^i\lambda^j \quad (4)$$

where $\alpha_{i,j}$ is the coefficient given in Table 1, The curve fit is a good approximation for values of $2 < \lambda < 13$. Values of λ outside this range represent very high and low wind speeds, respectively, that are outside the continuous rating of the machine (LV Dai, Tung, 2017; Miller et al., 2003).

Table 1: The coefficient of $\alpha_{i,j}$ for $i, j = 0, \dots, 4$.

i/j	0	1	2	3	4
0	-4.1909e-1	2.1808e-1	-1.2406e-2	-1.3365e-4	1.1524e-5
1	-6.7606e-2	6.0405e-2	-1.3934e-2	1.0683e-3	-2.3895e-5
2	1.5727e-2	-1.0996e-2	2.1495e-4	-1.4855e-4	2.7937e-6
3	-8.6018e-4	5.7051e-4	-1.0479e-4	5.9924e-6	-8.9194e-8
4	1.4787e-5	-9.4839e-6	1.6167e-6	-7.1535e-8	4.9686e-10

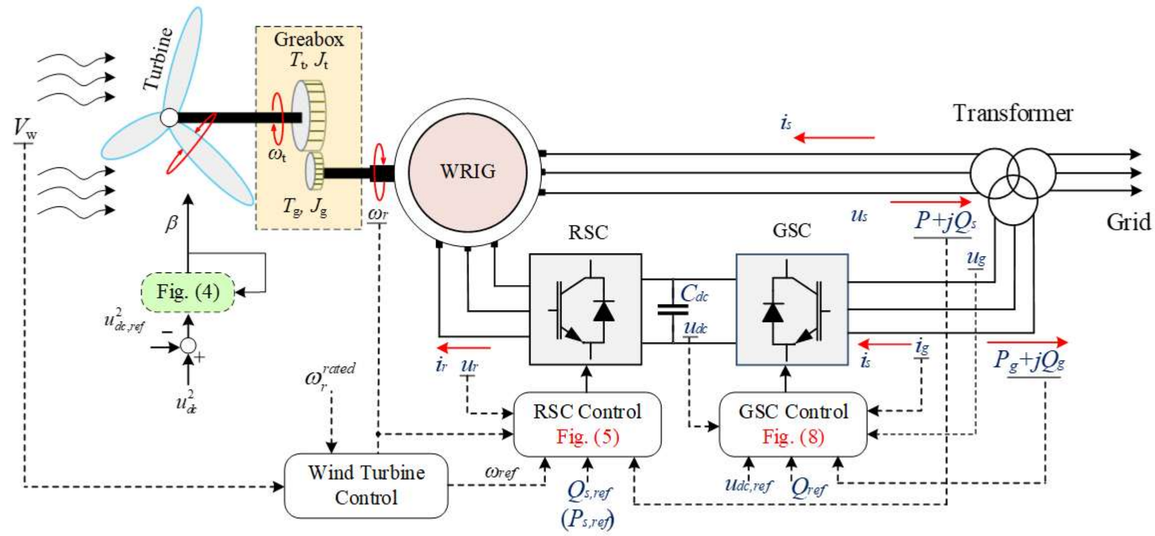

Figure 1. Block diagram of WECS

The turbine tip-speed ratio λ^{opt} is defined as:

$$\lambda^{opt} = \frac{\omega_t^{opt}}{V_w} R \quad (5)$$

Fig. 2 illustrates the variation of the power coefficient C_p concerning the tip speed ratio λ at different pitch angles. Observing this figure, the pitch angle is controlled at low to medium wind speeds to allow the WT to operate under optimal conditions. At high wind speeds, the pitch angle is adjusted to release some aerodynamic energy. WT are typically designed to harness the maximum possible wind energy at wind speeds ranging from 10 to

15 m/s. When wind speeds exceed 15 m/s, the turbine may shed some energy and will completely shut down at wind speeds reaching 20 to 25 m/s.

2.2. WRIG

The equivalent circuit of the DFIG-WECS is shown in Fig. 3-(a). For this study, the generator selected is the DFIG. Its mathematical expressions are formulated in the *dq*-axis reference frame of the synchronous rotating system and can be represented as (LV Dai & Tung, 2017; Jazaeri, Samadi, Najafi, & Noroozi-Varcheshme, 2012):

$$\begin{cases} u_d^s = R_s i_d^s - \omega\lambda_q^s + \dfrac{\partial \lambda_d^s}{\partial t} \\ u_q^s = R_s i_q^s + \omega\lambda_d^s + \dfrac{\partial \lambda_q^s}{\partial t} \end{cases} \tag{6}$$

$$\begin{cases} u_d^r = R_r i_q^r + (\omega - \omega_r)\lambda_d^r + \dfrac{\partial \lambda_q^r}{\partial t} \\ u_q^r = R_r i_d^r - (\omega - \omega_r)\lambda_q^r + \dfrac{\partial \lambda_d^r}{\partial t} \end{cases} \tag{7}$$

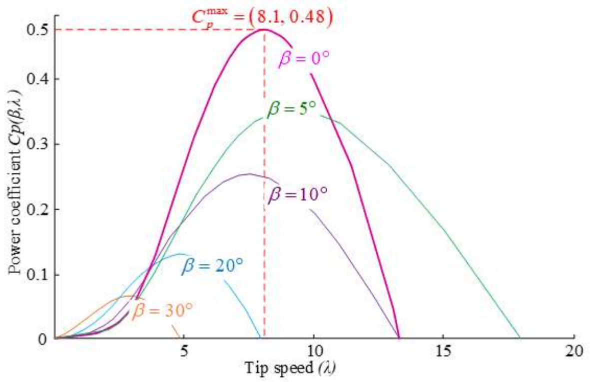

Figure 2. Power coefficient curves versus tip speed ratio for various pitch angles

Next, equations of magnetic flux of the rotor and stator:

$$\begin{cases} \lambda_d^s = \underbrace{(L_l^s + L_m)}_{L_s} i_d^s + L_m i_d^r \\ \lambda_q^s = \underbrace{(L_l^s + L_m)}_{L_s} i_q^s + L_m i_q^r \end{cases} \tag{8}$$

$$\begin{cases} \lambda_d^r = \underbrace{(L_l^r + L_m)}_{L_r} i_d^r + L_m i_d^s \\ \lambda_q^r = \underbrace{(L_l^r + L_m)}_{L_r} i_q^r + L_m i_q^s \end{cases} \tag{9}$$

According to Eqs. (6), (7), (8), and (9), the current equation can be rewritten under the following form:

$$\begin{cases} \chi \dfrac{\partial i_d^s}{\partial t} = -\dfrac{R_s i_d^s}{L_s} + \omega_r i_q^s + \dfrac{R_r L_m i_d^r}{L_s L_r} + \dfrac{\omega_r L_m i_q^r}{L_s} + \dfrac{u_d^s}{L_s} - \dfrac{L_m u_d^r}{L_s L_r} \\ \chi \dfrac{\partial i_q^s}{\partial t} = -\omega_r i_d^s - \dfrac{R_s i_q^s}{L_s} - \dfrac{\omega_r L_m i_d^r}{L_s} + \dfrac{R_r L_m i_q^r}{L_s L_r} + \dfrac{u_q^s}{L_s} - \dfrac{L_m u_q^r}{L_s L_r} \end{cases} \tag{10}$$

$$\begin{cases} \chi \dfrac{\partial i_d^r}{\partial t} = \dfrac{R_s L_m i_d^s}{L_s L_r} - \dfrac{\omega_r L_m i_q^s}{L_r} - \dfrac{R_r i_d^r}{L_s} - \dfrac{\omega_r L_m^2 i_q^r}{L_s L_r} + \dfrac{L_m u_d^s}{L_s L_r} - \dfrac{u_d^r}{L_r} \\ \chi \dfrac{\partial i_q^r}{\partial t} = \dfrac{\omega_r L_m i_d^s}{L_s} + \dfrac{R_s L_m i_q^s}{L_s L_r} + \dfrac{\omega_r L_m^2 i_q^r}{L_s L_r} - \dfrac{R_r i_q^r}{L_r} - \dfrac{L_m u_q^s}{L_s L_r} + \dfrac{u_q^r}{L_r} \end{cases} \tag{11}$$

where $\chi = (L_s L_r - L_m^2)/L_s L_r$, $\omega_r = p\omega_m$, u_d^s is the *d*-axis stator voltage, u_q^s is the *q*-axis stator voltage, u_d^r is the *d*-axis rotor voltage, u_q^r is the *q*-axis rotor voltage, i_d^s is the *d*-axis stator current, i_q^s is the *q*-axis stator current, i_d^r is the *d*-axis rotor current, i_q^r is the *q*-axis rotor current, R_s is the stator resistance, R_r is the rotor resistance, λ_d^s is the *d*-axis stator flux, λ_q^s is the *q*-axis stator flux, λ_d^r is the *d*-axis rotor flux, λ_q^r is the *q*-axis rotor flux, ω is the angular speed of the synchronously rotating reference frame, ω_r is the rotor angular speed, L_s is the stator inductance, L_r is the rotor inductance, L_l^s is the stator leakage inductance, L_l^r is the rotor leakage inductance, L_m is the mutual inductance, and p is the number of pole pairs.

Next, the active and reactive power outputs from the stator and rotor sides of the DFIG can be derived from Eqs. (6), (7), (8), and (9) and can be represented as follows:

$$\begin{cases} P_s = \left(u_d^s i_d^s + u_q^s i_q^s\right) \\ Q_s = \left(u_q^s i_d^s - u_d^s i_q^s\right) \end{cases} \quad \begin{cases} P_r = \left(u_d^r i_d^r + u_q^r i_q^r\right) \\ Q_r = \left(u_q^r i_d^r + u_d^r i_q^r\right) \end{cases} \tag{12}$$

Next, the total active and reactive power is:

$$\begin{cases} P_{total} = P_s + P_r \\ Q_{total} = Q_s + Q_r \end{cases} \tag{13}$$

Next, by ignoring rotor and copper losses, the active power of the rotor can also be represented by the following equation:

$$P_s = -sP_r \tag{14}$$

Finally, the equation of electromagnetic torque can be obtained as follows:

$$T_g = -\frac{1}{2} p L_m \left(i_q^s i_r^d - i_d^s i_q^r\right) \tag{15}$$

In this paper, when R_s, R_r, L_l^r and L_l^s and the alternating current (AC) components related to the type of impedance and reactance are ignored. This leads to the model not accurately reflecting the complex details. The stator resistance R_s and rotor R_r cause energy loss. The rotor L_l^r and stator L_l^s leakage currents cause the dynamic consequences of the current. When ignoring these parameters, from the formula (6) and (7) we rewrite as:

$$\begin{cases} u_d^s = -\omega \lambda_q^s \\ u_q^s = \omega \lambda_d^s \end{cases} \tag{16}$$

$$\begin{cases} u_d^r = \left(\omega - \omega_r\right) \lambda_d^r \\ u_q^r = -\left(\omega - \omega_r\right) \lambda_q^r \end{cases} \tag{17}$$

When the components R_s, R_r, L_l^r and L_l^s, are ignored, the electromagnetic torque T_e is calculated incorrectly, resulting in the actual mechanical speed ω_{mech} not fully reaching the optimum value ω_t^{opt}. This deviation can be described by:

$$\Delta\omega = \omega_t^{opt} - \omega_t \approx \frac{R_s + R_r}{L_l^s + L_l^r} \tag{18}$$

in which, the deviation ratio depends on the ratio between the resistance R_s, R_r and the total reactance L_l^r, L_l^s.

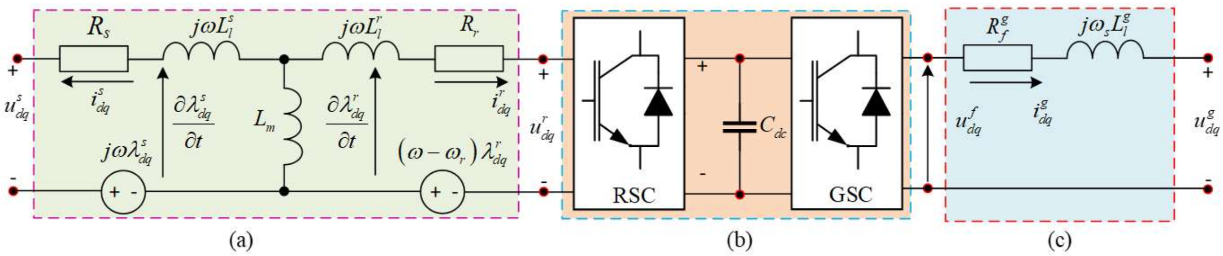

Figure 3. Equivalent circuit of DFIG; (a) WRIG generator, (b) Power electronic converters and DC link, (c) Grid filter

3. CONTROL STRATEGY

3.1. Wind Turbine Control

The pitch angle control adjusts the blade pitch when wind speeds exceed the rated value, limiting WT power output. As shown in Fig. 4,

$C_p^{\max}$ it reaches its maximum of 0.48 at a tip speed ratio $\lambda = 8.1$ and pitch angle $\beta = 0$. The mechanical torque driving the generator is given by Eq. (1) where (LV Dai & Tung, 2017; Liserre et al., 2011; Miller et al., 2003):

$$K = \frac{1}{2}\rho\pi R^2 C_p^{\max}(\lambda,\beta) \tag{19}$$

Therefore mechanical power can be obtained as follows (Yang et al., 2017):

$$\begin{aligned} P_m &= KV_w^3 \\ P_{out} &= P_w = T_w\omega_t \end{aligned} \tag{20}$$

The generator rotor reference speed is set as (Yang et al., 2017):

$$\omega_{r,ref} = \sqrt[3]{\frac{P_m}{K_{otp}}} = \sqrt{\frac{T_t}{K_{otp}}} \tag{21}$$

where $K_{otp} = (1/2)\left(R^2/\lambda_{otp}^3\right)\rho\pi C_p^{\max}(\beta,\lambda)$ is the optimal constant of the turbine is.

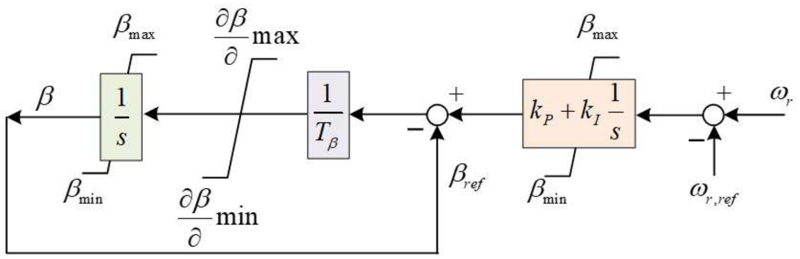

Figure 4. Schematic diagram of the pitch angle controller

3.2. WRIG Control

A. RSC control

The control diagram of the RSC is illustrated in Fig. 5, which includes inner and outer control loops. The outer control loop consists of two PI controllers, which are used to control the active power of the stator independently. Meanwhile, the inner control loop comprises two Fuzzy-PI controllers utilized to regulate the rotor current in the *d-q* axis independently.

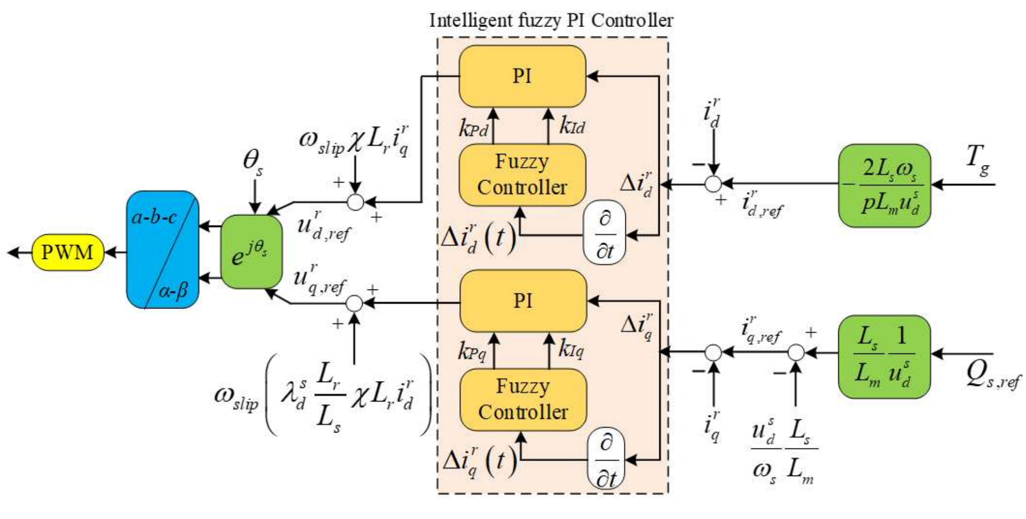

Figure 5. The control strategy of the RSC

To control the DFIG-WRIG, the *d*-axis of the synchronous reference frame is aligned with the stator flux, i.e. $\lambda_q^s = \lambda_r^s = 0$ or with the stator voltage, i.e. $u_q^s = 0$ Therefore, Eqs. (1) and (6)-(12) express the relationship between them i_q^r, i_d^r, ω_r and Q_s in the synchronously rotating reference frame with the *d*-axis directed along the stator flux, i.e. $\omega = \omega_s$, Assuming the stator flux is constant and neglecting the stator resistance as well as the damping factor, Eq. (12) yields:

$$\begin{cases} P_s = u_d^s i_d^s = u_d^s \left(-\frac{L_m}{L_s} i_d^r \right) \\ Q_s = -u_d^s i_q^s = u_d^s \left(\frac{u_d^s}{\omega_s L_s} + \frac{L_m}{L_s} \right) i_q^r \end{cases} \tag{22}$$

$$\begin{cases} P_r = u_q^r i_q^r = \omega_s \lambda_d^r i_q^r \\ Q_r = u_q^r i_d^r = \omega_s \lambda_d^r i_d^r \end{cases} \tag{23}$$

From Eq. (15), combined with the initial conditions, it can obtain as follows:

$$\begin{aligned} T_g &= \frac{p}{2}\left[\left(\lambda_q^s - L_m i_r^q \right) i_d^r - \left(\lambda_d^s - L_m i_r^d \right) i_q^r \right] \\ &= -\frac{p}{2} \frac{L_m}{L_s} \frac{u_d^s}{\omega_s} i_d^r \end{aligned} \tag{24}$$

From Eq. (22), it is evident that the stator active power P_s and electromagnetic torque T_g of the DFIG can be regulated by adjusting the i_d^r component of the rotor current. Similarly, the stator reactive power Q_s can be controlled through the i_q^r component. In essence, the d-axis rotor current influences the stator active power and torque, while the q-axis rotor current governs the stator flux and reactive power. Therefore, effective control of the DFIG can be achieved using these two decoupled components i_d^r and i_q^r, enabling us to meet the desired control objectives. The reference signals for control can be derived based on the required electromagnetic torque (or stator active power) and the desired stator reactive power, as outlined below:

$$\begin{cases} i_{d,ref}^r = -\frac{2}{p} \frac{L_s}{L_m} \frac{\omega_s}{u_d^s} T_g \\ i_{q,ref}^r = -\left(\frac{u_d^s}{L_s \omega_s} \frac{L_s}{L_m} \right) + \frac{L_s}{L_m u_d^s} Q_{s,ref} \end{cases} \tag{25}$$

Fuzzy controllers are widely used in industrial processes, especially when the system model is nonlinear or unavailable. This paper presents a fuzzy control system that adjusts PI controller parameters using fuzzy rules, making the adaptive PI controller nonlinear. Many studies develop these fuzzy controllers through experimental methods (Kenza, Lamia, Farid, & Mihai, 2024; Mohamed, Eskander, & Ghali, 2001; Phung, Wu, & Pham, 2024). Therefore, the PI expression is provided in the form of:

$$y(t) = k_P \Delta i(t) k_I \int_0^t \Delta i(t) \partial t \tag{26}$$

where $y(t)$ is the output of the control, $\Delta i(t)$ is the input of the control, k_P is the parameter of the scale, and the error between the reference current and the actual current is:

$$\begin{cases} \Delta i_d^r = i_{d,ref}^r - i_d^r \\ \Delta i_q^r = i_{q,ref}^r - i_q^r \end{cases} \tag{27}$$

The fuzzy control is based on control rules established from the input variables [NG, NM, NP, EZ, PP, PM, PG], which mean negative large, negative medium, negative small, zero, positive small, positive medium, and positive big, respectively. The control rules and membership functions are defined. The rules are listed as Rule 1, Rule 2, Rule 3, and Rule 4, each illustrated as shown in Fig. 6.

After the Fuzzy controller outputs the signal, it is fed into the PI controller for further refinement of the dq-axis voltage, so:

$$\begin{cases} u_{d,ref}^r = k_{Pd} \Delta i_d^r + k_{Id} \int_0^t \Delta i_d^r \partial t \\ u_{q,ref}^r = k_{Pq} \Delta i_q^r + k_{Iq} \int_0^t \Delta i_q^r \partial t \end{cases} \tag{28}$$

where k_{Pd} and k_{Pq} is the proportional gains of the PI controller, k_{Id} and k_{Iq} is the integral gains of the PI controller, and Δi_d^r, and Δi_q^r are the dq-axis current error. Then, the control signal from Eq. (28) is fed into the current controller to adjust the dq-axis voltage:

$$\begin{cases} i_d^r = \dfrac{u_d^r - \omega_{slip} L_r i_q^r}{R_r} \\ i_q^r = \dfrac{u_q^r - \omega_{slip} L_r i_d^r}{R_r} \end{cases} \tag{29}$$

where u_d^r và u_q^r are the output control voltage signals for the *dq*-axis.

Thus, the Fuzzy-PI controller enables precise adjustment of the system's current and rotor speed, optimizing operational efficiency and ensuring system stability under varying conditions. The rule surface diagram is shown in Fig. 7.

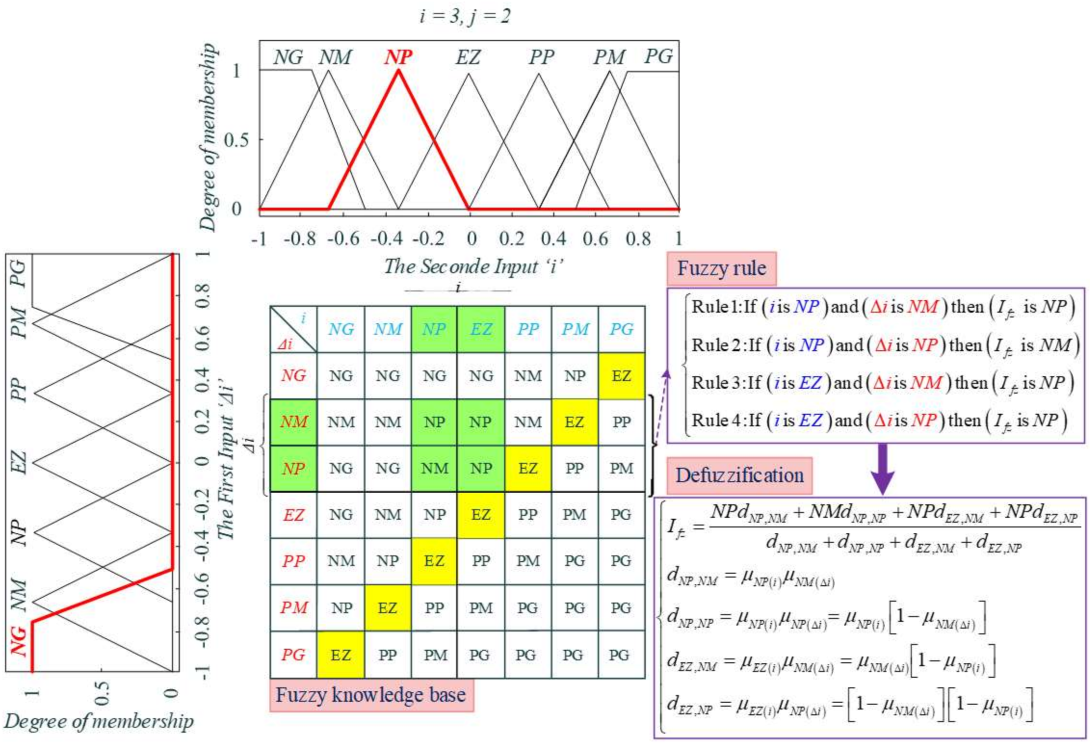

Δi \ i	NG	NM	NP	EZ	PP	PM	PG
NG	NG	NG	NG	NG	NM	NP	EZ
NM	NM	NM	NP	NP	NM	EZ	PP
NP	NG	NG	NM	NP	EZ	PP	PM
EZ	NG	NM	NP	EZ	PP	PM	PG
PP	NM	NP	EZ	PP	PM	PG	PG
PM	NP	EZ	PP	PM	PG	PG	PG
PG	EZ	PP	PM	PG	PG	PG	PG

$$I_f = \frac{NPd_{NP,NM} + NMd_{NP,NP} + NPd_{EZ,NM} + NPd_{EZ,NP}}{d_{NP,NM} + d_{NP,NP} + d_{EZ,NM} + d_{EZ,NP}}$$

$$\begin{cases} d_{NP,NM} = \mu_{NP(i)}\mu_{NM(\Delta i)} \\ d_{NP,NP} = \mu_{NP(i)}\mu_{NP(\Delta i)} = \mu_{NP(i)}\left[1-\mu_{NM(\Delta i)}\right] \\ d_{EZ,NM} = \mu_{EZ(i)}\mu_{NM(\Delta i)} = \mu_{NM(\Delta i)}\left[1-\mu_{NP(i)}\right] \\ d_{EZ,NP} = \mu_{EZ(i)}\mu_{NP(\Delta i)} = \left[1-\mu_{NM(\Delta i)}\right]\left[1-\mu_{NP(i)}\right] \end{cases}$$

Figure 6. The design of the fuzzy control

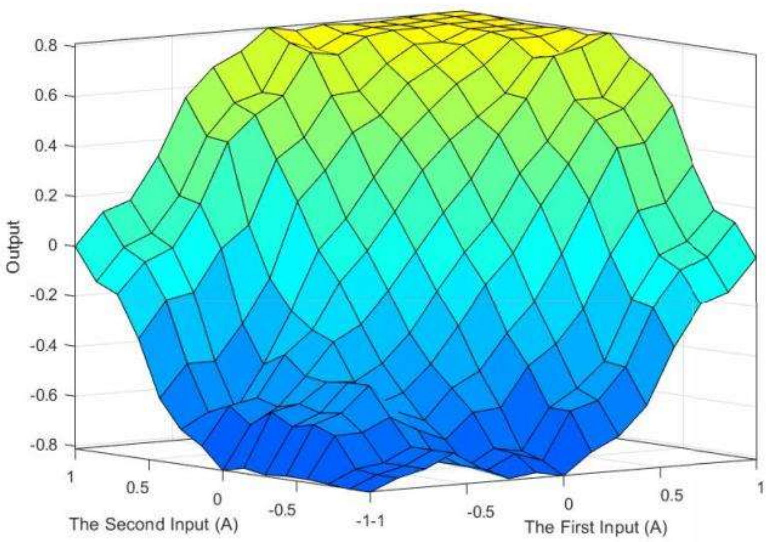

Figure 7. View plot surface of fuzzy controller

B. GSC control

The vector control method was applied to the GSC using a reference frame aligned with the grid voltage vector, allowing independent control of active and reactive currents. Like the RSC, the GSC uses PI controllers to regulate DC-link voltage, reactive power, and current, as shown in Fig. 8. The equivalent circuit of the grid filter is shown in Fig. 3-(c), with the voltage balance across described in the *dq* reference frame at ω_s.

$$\begin{cases} u_d^g = \left(R_f^g + \dfrac{\partial}{\partial t} L_f^g\right) i_d^g - \omega_s L_f^g i_q^g + u_d^f \\ u_q^g = \left(R_f^g + \dfrac{\partial}{\partial t} L_f^g\right) i_q^g + \omega_s L_f^g i_d^g + u_q^f \end{cases} \quad (30)$$

where R_f^g is the grid side filter resistance, L_f^g is the grid filter inductance, u_d^f is the *d*-axis grid filter voltage, u_q^f is the *q*-axis grid filter voltage, u_d^g is the *d*-axis grid voltage, u_q^g is the *q*-axis grid voltage, i_d^g is the *d*-axis grid filter current, i_q^g is the *d*-axis grid filter current and ω_s is the electrical angular speed of the grid voltage. Thus, the equivalent circuit of the DC-link is depicted in Fig. 3-(b). The following equation can describe the dynamic behavior of the capacitor (Krause, 2002; Pena, Clare, & Asher, 1996; Yang et al., 2017).

$$C_{dc} \frac{\partial}{\partial t} u_{dc} = i_{dc}^g - i_{dc}^r \quad (31)$$

where C_{dc} is the DC-link capacitance, u_{dc} is the DC-link voltage, the linear dynamic of the system is replaced by using the PI controller and can be expressed as:

$$C_{dc} \frac{\partial}{\partial t} u_{dc} = \left(k_{P_{dc}} + \frac{1}{s} k_{I_{dc}}\right)\left(u_{dc,ref} - u_{dc}\right) \quad (32)$$

$$L_f^g \frac{\partial}{\partial t} Q_g = \left(k_{P_{Q_g}} + \frac{1}{s} k_{I_{Q_g}}\right)\left(Q_{g,ref} - Q_g\right) \quad (33)$$

where $k_{P_{dc}}$ and $k_{I_{dc}}$ are the proportional and integral gains of the DC-link controller, $k_{P_{Q_g}}$ and $k_{I_{Q_g}}$ are the proportional and integral gains of the reactive power controller, respectively. Therefore, the *dq*-axis grid reference current can be obtained when passed through the proportional and integral gains; we have:

$$\begin{cases} i_{d,ref}^g = \dfrac{1}{\dfrac{2u_{d,ref}^g}{u_{dc}}} \left[A - \dfrac{3}{4} B - \dfrac{2u_{q,ref}^g}{u_{dc}} i_q^g \right] \\ i_{q,ref}^g = \dfrac{1}{R_f^g} \left[\dfrac{2}{3} \dfrac{1}{u_d^g} C - D \right] \end{cases} \quad (34)$$

with $A = \left(\dfrac{4}{3} C_{dc} \dfrac{\partial}{\partial t} u_{dc}\right)$, $D = u_{q,ref}^f + \omega_s L_f^g i_d^g$

$B = \left(\dfrac{2u_{d,ref}^r}{u_{dc}} i_d^r + \dfrac{2u_{q,ref}^r}{u_{dc}} i_q^r\right)$, $C = \left(L_f^g \dfrac{\partial}{\partial t} Q_g\right)$.

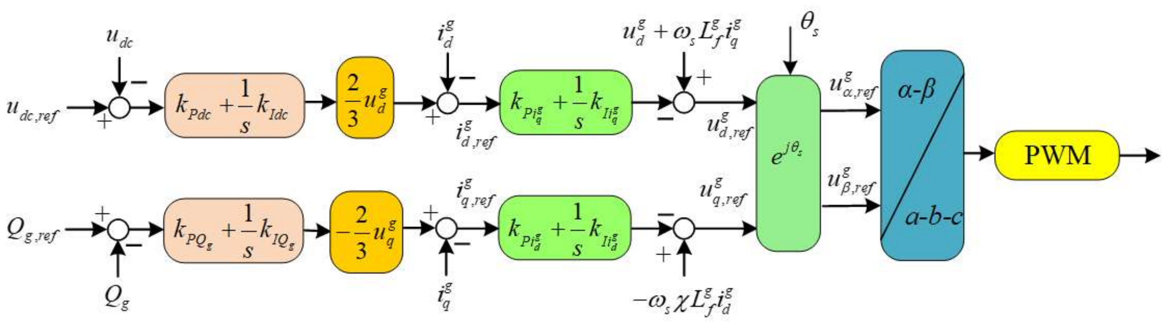

Figure 8. The control scheme of the GSC

4. CASE STUDIES AND RESULTS

To estimate the performance of the DFIG when combined with a WT, the system is simulated, as shown in Fig. 1, where the components are constructed using MATLAB/Simulink. The simulation parameters are provided in Table 2. During the simulation, V_w is set according to each case below. Assuming the gear ratio $GR = \omega_g / \omega_w$, the mechanical rotational speed of the DFIG is expected to reach ω_t^{rated}, while the mechanical rotational speed of the WT is scheduled to be ω_t^{opt} the simulation. In the simulation $Q_{s,ref}$, it decreases from the rated value to 0 at time t = 30 s and increases from 0 to $1.2Q_{s,ref}$ at time t = 60 s.

Table 2 Specifications of the studied DFIG and WT

Parameters		Value
The rated line voltage (RMS Value)	V_L	690 V
The rated frequency	f_{syn}	50 Hz
The poles	p	6
The full load slip	$s\%$	1
The moment of inertia	J	75 kg.m^2
The stator resistance	R_s	2.0 mΩ
The rotor resistance	R_r	1.5 mΩ
The stator leakage inductance	L_l^s	50 mΩ
The rotor leakage inductance	L_l^r	47 mΩ
The mutual inductance	L_m	860 mΩ
Swept area	A	3904 m^2
Density of air	ρ	1.2 kg/m^3
Rotor diameter	$2R$	70.5 m
System inertia	J_w	2.4×10^6 kgm^2

Case 1: Response to normal condition

An experiment testing the WT performance at a fixed wind speed of 10 m/s was selected as the reference condition to demonstrate the controller's responsiveness. The simulation results of the DFIG-WECS system, operating at this constant wind speed of 10 m/s, are presented in Fig. 9. From Figs 9-(a), (b), and (c), it can be observed that with a fixed wind speed of 10 m/s, the *dq*-axis rotor currents respond rapidly, generating control signals to regulate the generator torque, as shown in Fig. 9-(d), and to control the mechanical rotation speed of the WT as seen in Fig. 9-(e). Although the mechanical speed of the WT is controlled to remain stable under varying wind speeds, as illustrated in Fig. 9-(e), the mechanical speed of the DFIG does not consistently hold at the rated value, as depicted in Fig. 9-(f). Figs. 9-(g), (h), (i), and (j) show the active and reactive power of the generator. From Fig. 9-(i), we observe that in a steady state, P_{total} indicates that both the rotor and stator utilize the power produced by the WT. Additional cases will be examined by incrementally adjusting the wind speed in subsequent simulations to verify this observation.

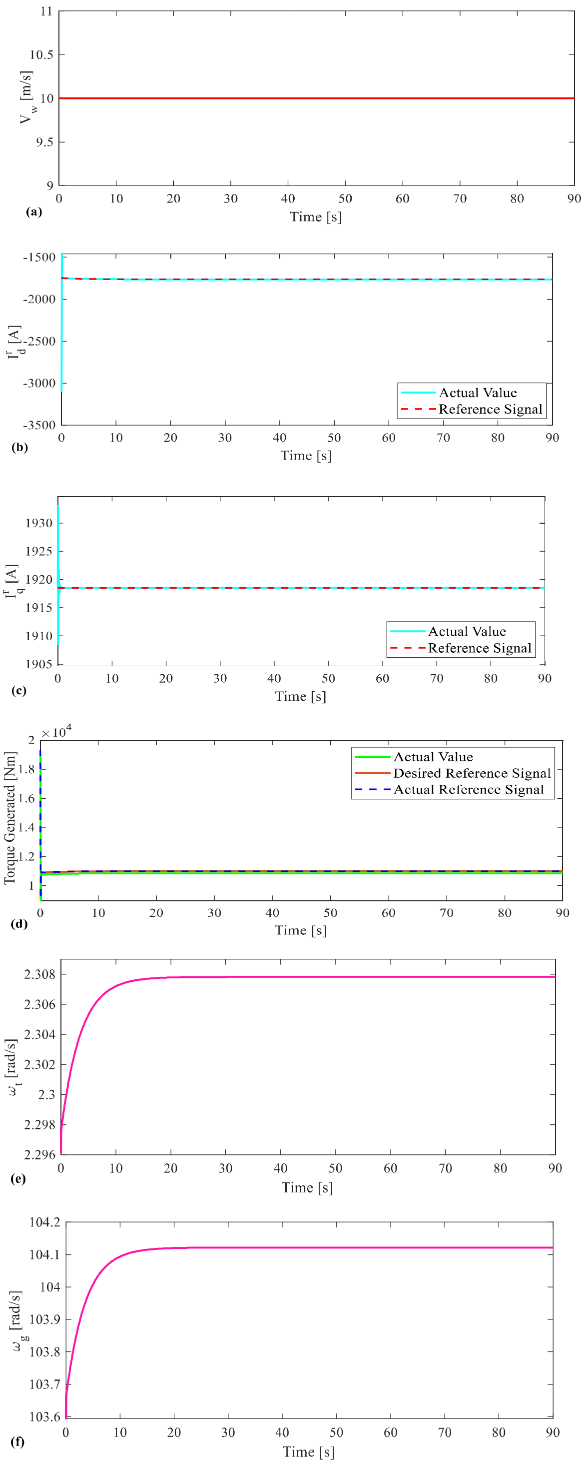

Figure 9. (*Cont*)

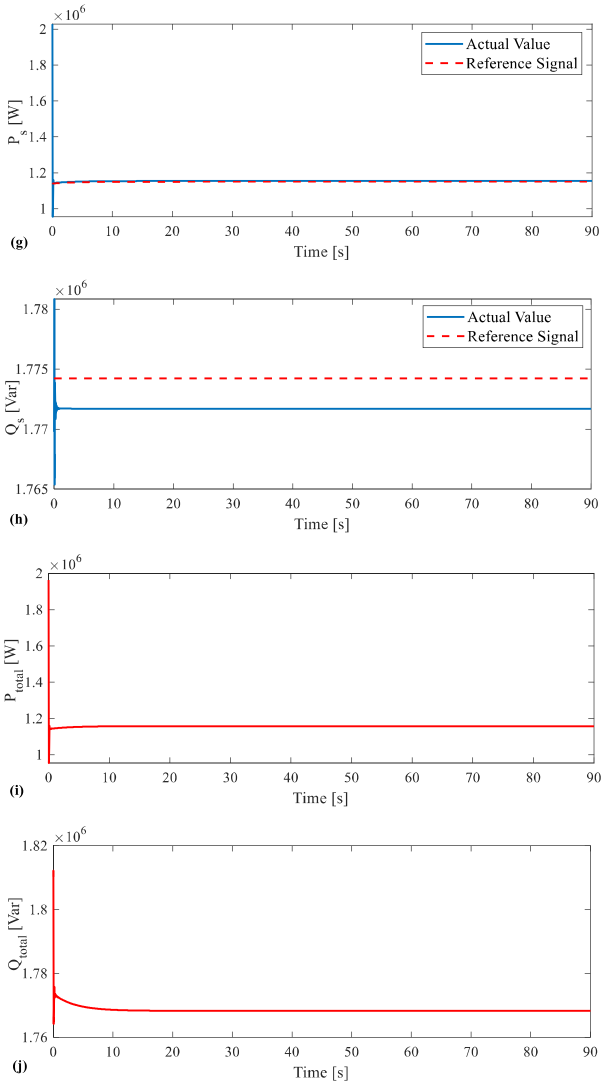

Figure 9. Response performance of DFIG-WECS under steady-state conditions; (**a**) Wind speed, (**b**) Rotor current *d*-axis, (**c**) Rotor current *q*-axis, (**d**) Torque Generated, (**e**) The WT mechanical speed, (**f**) The generator's mechanical speed, (**g**) Stator active power, (**h**) Stator reactive, (**i**) active power total, and (**j**) Reactive total

Case 2: A sudden increase in wind speed

In this simulation, $Q_{s,ref}$ are set to their rated value, while the wind speed V_w varies. The objective is for the control system to regulate the mechanical rotational speed of the WT ω_W so that the WT consistently operates at the desired speed. The simulation results are displayed in Fig. 10. Initially, V_w is set to 6 m/s, with both the DFIG and WT operating at rated speed. Then, V_w increases to 9 m/s at t = 30 s and 12 m/s at t = 60 s, as shown in Fig. 10-(a). The system quickly adjusts to observe the response of the *dq*-axis rotor currents under changing wind speeds, generating reference signals as shown in Figs. 10-(b) and (c) to control the generator torque, illustrated in Fig. 10-(f). The control signals and setpoints indicate a fast response to changes in wind speed.

From Fig. 10-(d), we observe that for V_w = *6 m/s* then $\omega_t^{opt} = 1.4\ rad/s$, the system is stable; with V_w = *9 m/s* then $\omega_t^{opt} = 2.062\ rad/s$, it remains stable; and at V_w = *12 m/s* then $\omega_t^{opt} = 2.751\ rad/s$, it again reaches a steady state. Figs. 10-(g), (h), (i), and (j) depict the active and reactive power of the generators. In Fig. 10-(i), we see that $P_w \approx P_s + P_r$, where P_w represents the actual output power of the WT, and P_s and P_r are the active power contributions from the generator's stator and rotor, respectively. This indicates that the WT output power is shared between the stator and rotor.

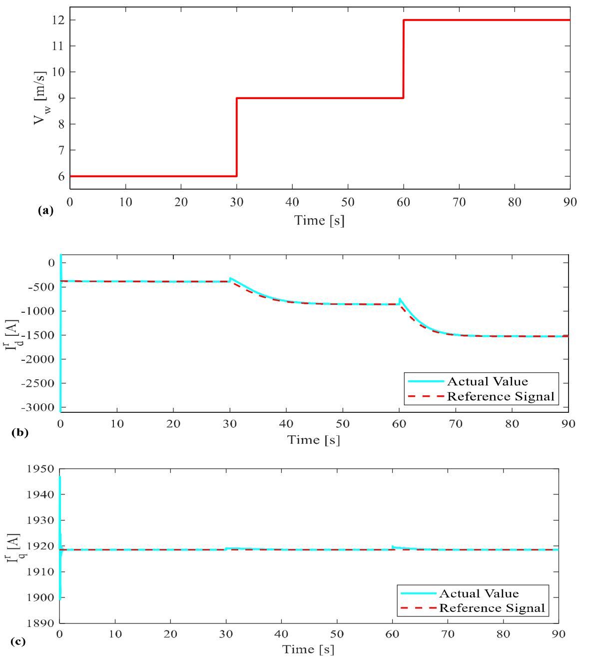

Figure 10. (*Cont*)

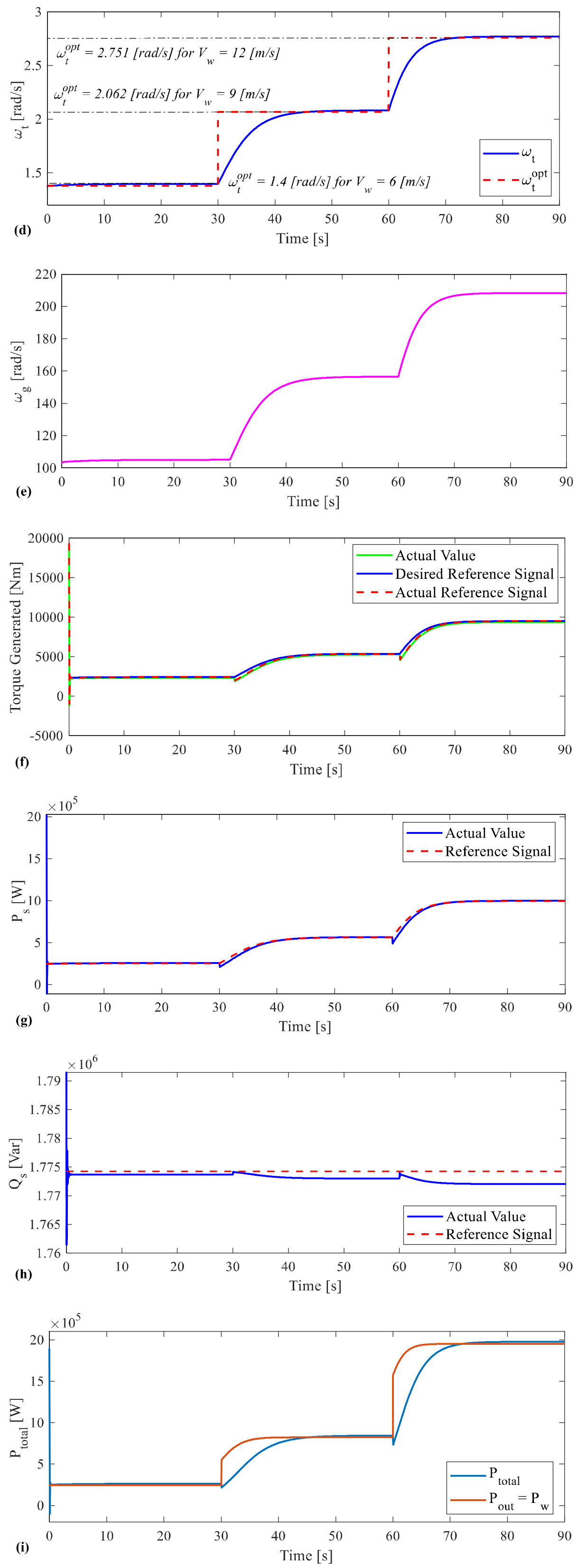

Figure 10. (*Cont*)

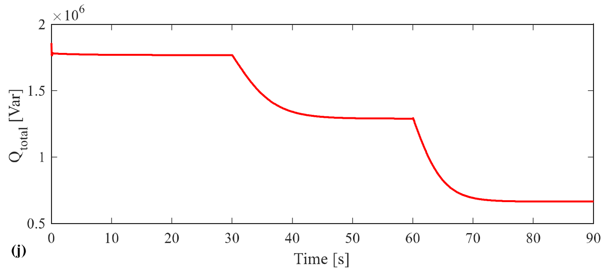

Figure 10. Response performance of DFIG-WECS under steady-state conditions; (**a**) Wind speed, (**b**) Rotor current *d*-axis, (**c**) Rotor current *q*-axis, (**d**) The WT mechanical speed, (**e**) The generator's mechanical speed, (**f**) Torque Generated, (**g**) Stator active power, (**h**) Stator reactive, (**i**) Active power total, and (**j**) Reactive total.

Case 3: A sudden decrease in wind speed

Once again, we observe that wind speed changes from 12 m/s to 9 m/s at t = 30 s and then decreases to 6 m/s at t = 60 s. The simulation results are shown in Figure 11. From Figs. 11-(b) and (c), we can see that the d-axis rotor current consistently tracks the setpoint, and the generator torque displayed in Fig. 11-(f) also demonstrates a fast response and accurate tracking of the setpoint with changes in wind speed. Regarding power, we can observe a rapid response returning to the reference value, as illustrated in Fig. 11-(i). Additionally, we can see that in the steady-state $P_w \approx P_s+P_r$. This indicates that the power generated by the WT is consumed by both the rotor and the stator. From Fig. 11-(d), it can be observed that with V_w = *12 m/s*, $\omega_t^{opt} = 2.769\ rad/s$ the system is in steady-state; with V_w = *9 m/s*, $\omega_t^{opt} = 2.086\, rad/s$ the system is in steady-state, and with V_w = *6 m/s* then $\omega_t^{opt} = 1.398\ rad/s$. The system is in a steady state. Therefore, based on the simulation results, it has been demonstrated that the designed controllers can effectively control the DFIG and automatically adjust the rotor voltage applied to it, enabling the WT to operate under optimal conditions.

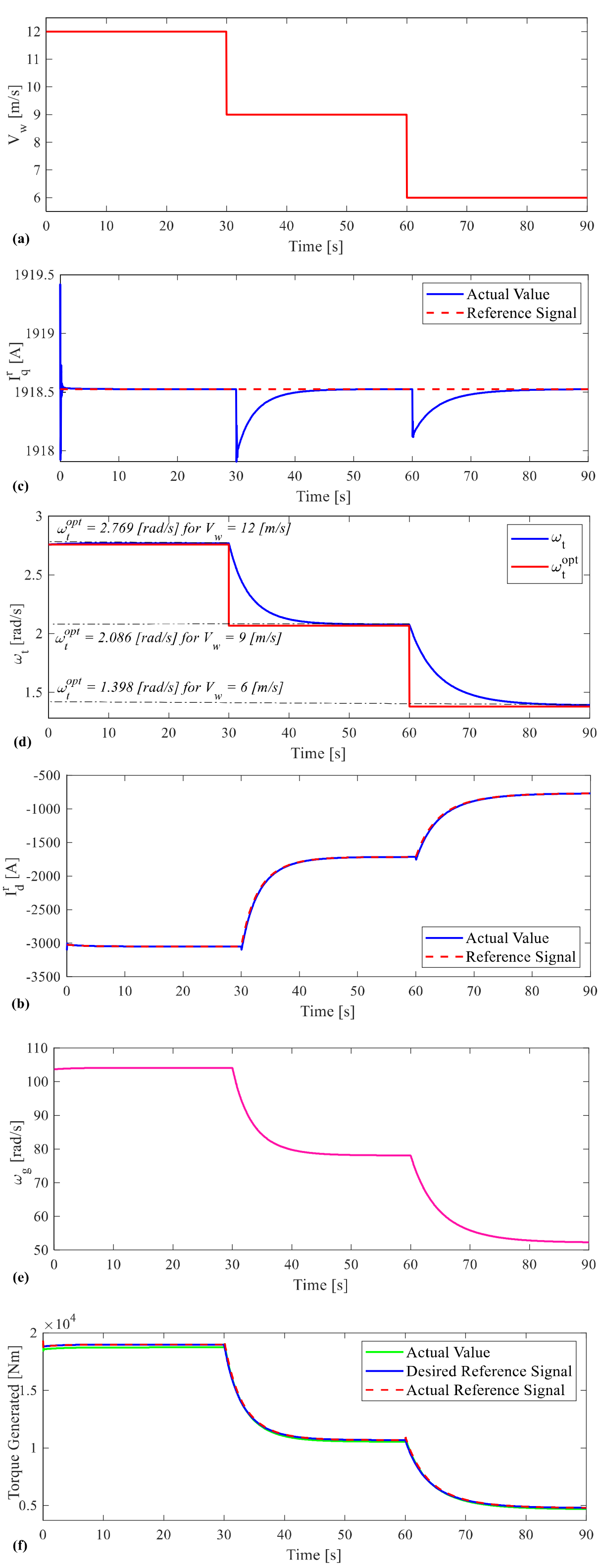

Figure 11. (*Cont*)

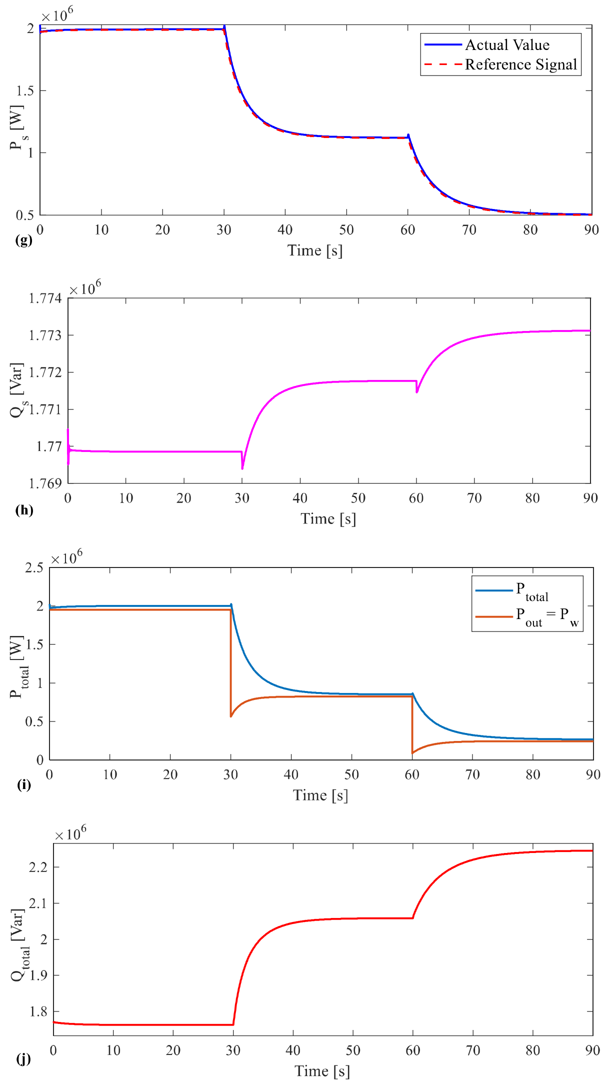

Figure 11. Response performance of DFIG-WECS under steady-state conditions; (**a**) Wind speed, (**b**) Rotor current *d*-axis, (**c**) Rotor current *q*-axis, (**d**) The WT mechanical speed, (**e**) The generator's mechanical speed, (**f**) Torque Generated, (**g**) Stator active power, (**h**) Stator reactive, (**i**) Active power total, and (**j**) Reactive total

5. CONCLUSION

This paper presents a feasible and efficient control strategy for the rotor-side converter of a DFIG, fully leveraging the inherent properties of wind turbine generator systems. The control scheme utilizes vector control techniques; the PI controller is designed based on Fuzzy logic, and the entire model is developed in MATLAB/Simulink.

From the simulation cases, it can be concluded that the proposed model is a helpful simulation tool for experimental purposes, modeling, research, and performance analysis of the system under varying DFIG parameters and wind speeds. The proposed Fuzzy-PI controller demonstrated excellent dynamic performance, ensuring high power quality even with wind speed fluctuations. The results indicate that the mechanical rotational speed of the WT can approach the optimal speed. However, a slight deviation remains due to excluding parameters such as R_s, R_r, L_l^r and L_l^s the DFIG modeling process. Therefore, a subsequent recommendation of this paper is to minimize the discrepancy between the ideal and actual rotational speed by carefully considering parameters like R_s, R_r, L_l^r and L_l^s the DFIG-WECS model.

REFERENCES

Abolhassani, M. T., Enjeti, P., & Toliyat, H. (2008). Integrated doubly fed electric alternator/active filter (IDEA), a viable power quality solution, for wind energy conversion systems. *IEEE Transactions on Energy Conversion, 23*(2), 642-650.

Ackermann, T. (2012). *Wind power in power systems*: John Wiley & Sons.

Bensahila, B., Allali, A., Merabet Boulouiha, H., & Denai, M. (2020). Modeling, Simulation and Control of a Doubly-Fed Induction Generator for Wind Energy, Conversion Systems. *International Journal of Power Electronics and Drive Systems (IJPEDS)*.

Boutoubat, M., Mokrani, L., & Machmoum, M. (2013). Control of a wind energy conversion system equipped by a DFIG for active power generation and power quality improvement. *Renewable Energy, 50*, 378-386.

Dai, L., & Pham, H. T. (2023). A Feasible MPPT Algorithm for the DC/DC Boost Converter: An Applied Case for Stand-Alone Solar Photovoltaic Systems. *International journal of electrical and computer engineering systems, 14*(6), 713-724.

Dai, L., & Tung, D. (2017). Modeling for Development of Simulation Tool: A Case Study of Grid Connected Doubly Fed Induction Generator Based on Wind Energy Conversion System. *International Journal of Applied Engineering Research, 12*(11), 2981-2996.

Hassan, Q., Viktor, P., Al-Musawi, T. J., Ali, B. M., Algburi, S., Alzoubi, H. M., . . . Jaszczur, M. (2024). The renewable energy role in the global energy Transformations. *Renewable Energy Focus, 48*, 100545.

Jain, A. K., & Ranganathan, V. (2008). Wound rotor induction generator with sensorless control and integrated active filter for feeding nonlinear loads in a stand-alone grid. *IEEE Transactions on Industrial electronics, 55*(1), 218-228.

Jazaeri, M., Samadi, A., Najafi, H., & Noroozi-Varcheshme, N. (2012). Eigenvalue Analysis of a Network Connected to a Wind Turbine Implemented with a Doubly-Fed Induction Generator (DFIG). *Journal of applied research and technology, 10*(5), 791-811.

Kenza, M., Lamia, Y., Farid, N., & Mihai, C. (2024). *Fuzzy Based Vector Control Strategy for a Doubly Fed Induction Motor*. Paper presented at the 2024 12th International Conference on Smart Grid (icSmartGrid).

Krause, P. (2002). Analysis of Electric Machinery and Drive Systems. *IEEE Press google schola, 2*, 203-210.

Liserre, M., Cardenas, R., Molinas, M., & Rodriguez, J. (2011). Overview of multi-MW wind turbines and wind parks. *IEEE Transactions on Industrial electronics, 58*(4), 1081-1095.

Mehdipour, C., Hajizadeh, A., & Mehdipour, I. (2016). Dynamic modeling and control of DFIG-based wind turbines under balanced network conditions. *International Journal of Electrical Power & Energy Systems, 83*, 560-569.

Miller, N. W., Price, W. W., & Sanchez-Gasca, J. J. (2003). Dynamic modeling of GE 1.5 and 3.6 wind turbine-generators. *GE-Power systems energy consulting*(3.0).

Mohamed, A. Z., Eskander, M. N., & Ghali, F. A. (2001). Fuzzy logic control based maximum power tracking of a wind energy system. *Renewable Energy, 23*(2), 235-245.

Pena, R., Clare, J., & Asher, G. (1996). Doubly fed induction generator using back-to-back PWM converters and its application to variable-speed wind-energy generation. *IEE Proceedings-Electric power applications, 143*(3), 231-241.

Phung, B. N., Wu, Y.-K., & Pham, M.-H. (2024). Novel Fuzzy Logic Controls to Enhance Dynamic Frequency Control and Pitch Angle Regulation in Variable-Speed Wind Turbines. *Energies, 17*(11), 2617.

Singh, M., & Chandra, A. (2010). Application of adaptive network-based fuzzy inference system for sensorless control of PMSG-based wind turbine with nonlinear-load-compensation capabilities. *IEEE transactions on power electronics, 26*(1), 165-175.

Tohidi, A., Abedinia, O., Bekravi, M., & Ojaroudi, N. (2016). Multivariable adaptive variable structure disturbance rejection control for DFIG system. *Complexity, 21*(4), 50-62.

Yang, X., Liu, G., Li, A., & Le, V. D. (2017). A predictive power control strategy for DFIGs based on a wind energy converter system. *Energies, 10*(8), 1098.

MỘT CHIẾN LƯỢC ĐIỀU KHIỂN MỚI NHẰM NÂNG CAO ĐÁP ỨNG ĐỘNG CỦA HỆ THỐNG CHUYỂN ĐỔI NĂNG LƯỢNG GIÓ SỬ DỤNG MÁY PHÁT ĐIỆN CẢM ỨNG NGUỒN KÉP DỰA TRÊN BỘ ĐIỀU KHIỂN FUZZY-PI

Nguyễn Thị Huệ[1], Huỳnh Hoàng Bảo Nghĩa[2], Lê Văn Đại[2*]

[1]*Trường Đại học Công nghệ Đồng Nai*

[2]*Trường Đại học Công nghiệp Thành Phố Hồ Chí Minh*

*Tác giả liên hệ: *Lê Văn Đại, levandai@iuh.edu.vn*

THÔNG TIN CHUNG

Ngày nhận bài: 10/11/2024

Ngày nhận bài sửa: 03/01/2025

TÓM TẮT

Bài báo này giới thiệu phương pháp điều khiển công suất hiệu quả và đơn giản cho hệ thống chuyển đổi năng lượng gió dựa trên

Ngày duyệt đăng: 08/01/2025

TỪ KHOÁ

Bộ điều khiển tỷ lệ tích phân;

Máy phát điện cảm ứng nguồn kép ;

Mờ hóa;

Mô phỏng

Hệ thống chuyển đổi năng lượng gió;

Đáp ứng động.

máy phát điện cảm ứng nguồn kép. Do hiệu suất bị hạn chế bởi bộ điều khiển tỷ lệ tích phân truyền thống khi thay đổi các thông số của máy phát điện cảm ứng nguồn kép và tốc độ gió, vì vậy lý thuyết điều khiển mờ hóa được áp dụng để khắc phục những hạn chế này. Đầu tiên, một mô hình toán học chi tiết của máy cảm ứng trong miền *dq* được cung cấp. Sau đó, dựa trên các đặc tính của máy phát điện cảm ứng nguồn kép, một mô hình toán học cải tiến được trình bày cùng với mô hình điều khiển véc tơ cho máy phát điện. Sau đó, mô hình toán học cho tuabin gió và bộ điều khiển mờ hoá được xây dựng dựa trên bộ điều khiển tỷ lệ tích phân và được triển khai trên phần mềm Matlab/Simulink để mô phỏng và đánh giá hiệu suất của bộ điều khiển. Kết quả mô phỏng chỉ ra rằng việc điều khiển máy phát điện cảm ứng cấp nguồn kép bằng phương pháp đề xuất có thể cải thiện đáng kể hiệu suất đáp ứng động khi chịu các tác nhân thay đổi thông số máy phát và tốc độ gió khác nhau.